Materials Science & Engineering B 236–237 (2018) 189–196

Contents lists available at ScienceDirect

Materials Science & Engineering B

journal homepage: www.elsevier.com/locate/mseb

Revealing of ultrasonic wire bonding mechanisms via metal-glass bonding

Yangyang Long[a,*], Folke Dencker[b], Andreas Isaak[b], Chun Li[a], Friedrich Schneider[c], Jörg Hermsdorf[c], Marc Wurz[b], Jens Twiefel[a], Jörg Wallaschek[a]

[a] Institute of Dynamics and Vibration Research, Leibniz Universität Hannover, Appelstr. 11, 30167 Hanover, Germany
[b] Institute of Micro Production Technology, Leibniz Universität Hannover, An der Universität 2, 30823 Garbsen, Germany
[c] Laser Zentrum Hannover e.V., Hollerithallee 8, 30419 Hanover, Germany

ARTICLE INFO

Keywords:
Ultrasonic bonding mechanisms
Real-time observation
Microwelds area
Oxide particle movement

ABSTRACT

Very complex phenomena and interface changes occur during the ultrasonic wire bonding process, which lead to an incomplete understanding of the process, especially for the friction and softening phases. In this work, the bonding process was real-time observed via metal-glass bonding to achieve a deeper understanding of these phenomena. Through the 2D high-speed observation, the emergence and changes of five areas including the contact area, friction area, stick area, microwelds area and oxides area were observed and quantified. The stick and microwelds area were observed to start from the central region and extend outwards. Normal force and ultrasonic power interactively influence these areas. The moving of oxides was captured and confirmed to be caused by both the material flow and vibration. The ultimate shear stress of microwelds was calculated to be 95.72 MPa with which the quantification of the observed microwelds area can be used to predict the bonding strength.

1. Introduction

The ultrasonic (US) wire bonding technology which applies normal force and US vibration to produce high reliable interconnections was invented in the 1960s [1]. Since then, the microelectronic interconnection market has been dominated by this technique. During the ultra-short process (tens to hundreds of milliseconds depending on the wire diameter and material), very complicated physical phenomena occur at the wire/substrate interface. Due to the dynamic changes of these phenomena, the short process time and the enclosed interface, a good understanding of the underlying mechanisms is still lacked after decades of usage.

According to state-of-the-art knowledge [2], the bonding process can be divided into four phases: 1) Pre-deformation and activation of US vibration, 2) Friction, 3) US softening and 4) Interdiffusion. During the first phase, the wire is first plastically deformed due to the normal force. The US vibration is activated but the wire still sticks on the substrate as long as the vibration amplitude is not big enough. When the amplitude exceeds a threshold value, friction between the wire and the substrate starts. During the softening phase, continuous plastic deformation takes place and microwelds are formed. Interdiffusion takes place once a microweld is formed. The geometry changes of the wire caused by pre-deformation and the softening induced macroscopic deformation have been extensively studied [3–5], especially at z-dimension. The activation of US vibration and the friction have been investigated by micro-sensors [6], laser vibrometers [3,7,8] and real-time observations [9–12]. The existence of relative motions at both the wire/substrate interface and the wire/tool interface were validated by these studies. By analyzing the element distributions at different process times, it was shown that the relative displacement amplitudes at different locations of the wire/tool interface are different [13]. A detailed investigation on the variations of relative motion at different locations of the wire/substrate interface, however, has not been conducted, especially in a real-time manner. The microwelds [14–16] as well as interdiffusion [17–19] can only be indirectly measured or observed by wire removal or cross-cut when the bonding process is terminated. The switch from friction to microwelds connection at different locations of the wire/substrate interface has not been studied as well. Maeda et al. [20,21] tried to record the expansion of the wire/substrate contact area through a transparent glass but at a low frame rate. In conclusion, these complicated phenomena taking place at the two-dimensional wire/substrate interface has not yet been observed and measured in real-time from a 2-D point of view.

In this work, the wire/substrate interface is directly observed by using a transparent glass substrate instead of the commonly used metallization substrate. By using a high-speed observation system, all the

* Corresponding author.
E-mail address: long@ids.uni-hannover.de (Y. Long).

https://doi.org/10.1016/j.mseb.2018.11.010
Received 19 September 2017; Received in revised form 5 October 2018; Accepted 23 November 2018
Available online 29 November 2018
0921-5107/

phases mentioned above except interdiffusion can be real-time observed and quantified. The interfaces after the mechanical removal of the wire were observed by Scanning Electron Microscope (SEM). Even though metal-glass joining mechanism (both metallic bonds and ionic bonds can exist) is different from that of metal-metal joining (only metallic bonds), they are still similar since both processes involve Pre-deformation and activation of US vibration phase, Friction phase and Softening phase and undergo the phenomena of relative motion, oxide removal and microwelds formation. As a result, the knowledge gained from the metal-glass bonding is beneficial to understand the common metal-metal wire bonding process.

2. Experiments

The aluminum wire used in this work is Al-H11 obtained from Heraeus GmbH. The diameter of the thick wire is 400 μm and it possesses a breaking load of 500–700 cN at more than 5% elongation. The thick aluminum wire bonding head HBK05 is provided by Hesse Mechatronics GmbH. The natural frequency of the transducer in the bonding head is around 60 kHz and is driven by an in-house developed digital phase controller [22] together with a Bruel & Kjær 2713 amplifier. The transparent silica glass with a dimension of 40 × 40 × 3 mm and a surface roughness of less than 1.2 nm is ordered from Siegert Wafer GmbH.

The physical phenomena during the bonding process were observed by a high speed observation system consisting of a high speed camera and a magnification system. The high speed camera Phantom v710 was obtained from Vision Research Inc. The pixels on the CMOS sensor of the camera have a size of 20 × 20 μm. Due to the relatively large pixel size, a reverse lens technique is applied to enhance the resolution. A C-Mount 12.5 mm Pentax lens is connected with a bellow to constitute the magnification system. With an 18× magnification system, a resolution of 1.1 μm/pixel is reached. Due to the limited data writing speed of the camera, a trade-off between the window size and the frame rate has to be made to record the bonding process. The window size used in this work was 640 × 480 pixel and the corresponding frame rate was 20,000 fps. Even though the frame rate was smaller than the bonding frequency, the videos are able to record the details of the bonding process due to the phase difference between the vibration and the recording rate. The sharpness of the videos was assured by an exposure time of 2 μs. The whole observation system is vertically installed underneath the bonding platform. To provide enough light onto the tiny recording area (704 × 528 μm) within the extremely short exposure period, a laser source JOLD-45-CPXF-1P from Jenoptik AG was applied.

3. Results and discussion

3.1. Real-time observation

The video (it can be found in the Supplementary material) was first taken under the setting of 5 N normal force, 2.4 W US power and 400 ms process time. The first phenomenon that can be observed is the change of the wire/substrate contact. During the Pre-deformation stage, the line contact became an elliptic area contact under the normal force. The US vibration was then applied and the driving current of the transducer throughout the bonding process is shown in Fig. 1. From the data of the driving current, it can be calculated that the whole bonding process lasted for 0.3998 s. The video contains, however, only 7962 frames which correspond to 0.3981 s. This means that in the first ~1 ms when the vibration amplitude of the tool tip was too small, the wire was stuck on the glass and only elastic deformation of the wire took place, which is in accordance to [3]. The same situations took place during the last ~1 ms of the process.

In the meantime, the elliptic contact area started to expand within the softening phase. Once the US vibration amplitude was big enough to overcome the maximum static friction force, the friction between the wire and the substrate was observed. Since the sliding between the wire and the substrate in the peripheral contact region was more severe, the peripheral region of the contact first became bright. The high brightness was caused by the breakage of the aluminum oxides into small particles. Since they have many facets with different angles, the particles can reflect more light into the observation system than the original oxides in the form of flakes, which is confirmed in [23]. As US vibration continued, the bright areas extended to the central region until the whole contact region was covered by the bright layer (oxide particles). The distribution of the bright area represents different relative displacement amplitudes at different locations of the wire/substrate interface, as shown in Fig. 2. The wire is the dark area, as marked in the red rectangle in Fig. 2(a). Due to the larger relative displacement amplitude compared to that in the central region, the oxides in the peripheral contact region were first broken into small particles and the corresponding region in Fig. 2(b) exhibited a high brightness. At the moment Fig. 2(c) captured, the oxides in the whole contact area were broken into small particles. As the bonding tool is symmetric, the contact area in Fig. 2(c) is also symmetric with respect to the middle horizontal line of the image. When the tool tip surface was not parallel to the substrate surface, however, the contact area became asymmetric. And in this case, the bright area started from one side of the peripheral contact region instead of the whole peripheral contact region. The friction continued until microwelds formed. During the friction phase, the natural oxides covered on the pure metal surface was detached, broken up into small particles and transported outwards. To make the oxide removal process faster, a larger vibration amplitude in the beginning stage of bonding process is recommended.

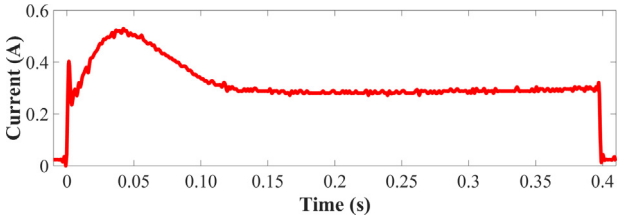

Fig. 1. Driving current of the transducer under 5 N 2.4 W.

According to Blaha and Langenecker [24,25], when the vibration amplitude exceeds a threshold value, the acoustic waves push the dislocations within the crystals out of their pinned positions so that the yield stress of the material is lowered. Additionally, the vibration superimposes additional oscillatory stress on the wire. Consequently, a macroscopic continuous plastic deformation of the wire occurs and results in a larger contact area, which was clearly shown by the series of images in Fig. 2. The expansion rate in the beginning of the softening phase was high and became lower in the latter stage. The quantification of the contact area over the process time will be shown later. By the combination effect of the continuous plastic deformation induced material flow and the US vibration induced reciprocal motion, the oxides were continuously transported to the peripheral region of the contact. This will be discussed later.

As shown in Fig. 2(d–f), another dark area formed in the central region. It started at ~109 ms and extended until ~208 ms. This newly formed stick area showed the static state of the central part of the wire while the other part of the wire surrounding this stick area still slid on the glass, which can be clearly observed in the video. Before the emergence of the stick area, the vibration amplitude at this area became smaller and smaller, as indicated from obvious vibration to blinking in the video. The blinking was due to the resolution of the observation system (1.1 μm). Once the stick area extended to the surrounding sliding area, the sliding at the surrounding area stopped immediately. This implies the formation of microwelds which prevented the sliding of the corresponding part of the wire. In the mean time of the stick area expansion, the outwards moving of oxides can be observed. And during

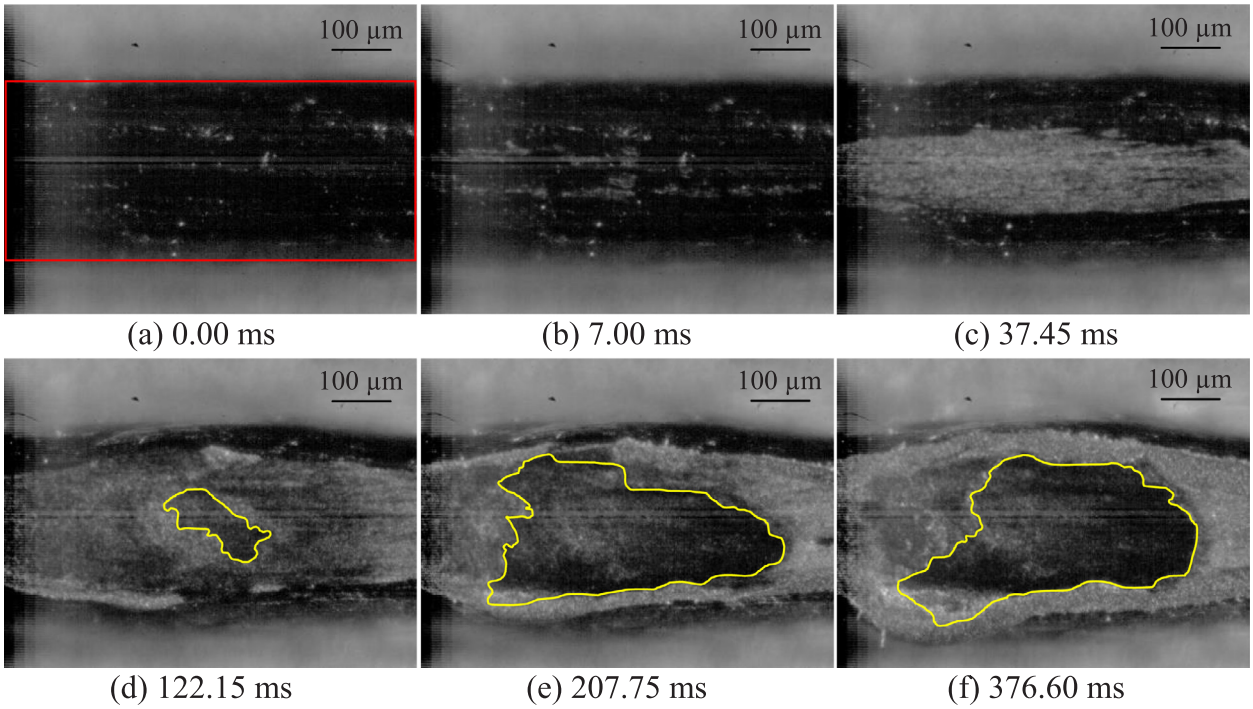

Fig. 2. Selected images from the recorded process under 5 N 2.4 W.

the moving, some oxides as indicated by their high brightness retained within the stick area. Therefore, the stick area consists of microwelds areas and oxides areas which can be distinguished by their brightness. Due to the extremely small roughness (Ra: 1.2 nm) of the glass surface, the oxides left within the stick area covered the asperities and inhibited the formation of microwelds. After ~208 ms as shown in Fig. 2(f), the stick area in the upper-left region became smaller, which indicates the breakage of the existing microwelds caused by excessive US vibration [26,27]. Therefore, a small vibration amplitude is recommended in the later stage of bonding processes. As more area in the upper-right contact region became static, the stick area in total was not significantly changed.

3.2. SEM observation

After the bonding process, the wire was mechanically removed by a shear tester and the wire/glass interface was then observed by SEM. Fig. 3 shows the bonding interface under 5 N 1.3 W. Fig. 3(a) was the last frame subtracted from the high-speed video. It can be clearly seen that the stick area in the video (as marked in the yellow borders in Fig. 3(a)) fits the aluminum residual in Fig. 3(b) very well, which indicates that this area was well bonded. Even though certain amount of oxides left in the stick area, the microwelds among the oxides were strong enough to keep the aluminum residual during the mechanical removal of the wire. The aluminum residual was then etched off by peroxymonosulfuric acid (H_2SO_5) and the surface roughness of the glass underneath the residual was measured to be Ra 1.24 nm which is similar to that before bonding. This indicates that the bonding process did not cause severe wear within the stick area. The two ends areas as shown in Fig. 3(c) are almost free of oxides. On one hand, this could be partially caused by the removal of wire during which the oxides were removed simultaneously. On the other hand, this indicates that only a small amount of oxides left within the inner contact region. Fig. 3(d) corresponding to the bright peripheral region in Fig. 3(a), shows that most oxides were transported to this region, which represented the effective oxide removal process within the metal residual region.

Different from the wire removal of 5 N 1.3 W, the wire removal for 6 N 2.1 W caused the fracture of the glass, as shown in Fig. 4. In this case, the stick area as marked in the yellow border cannot be compared to the SEM image where there is no indication for the bonded area. The fracture traces in Fig. 4(b), however, indicates a high bonding strength. The peripheral region outside of the yellow border in Fig. 4(a) was assumed not to be well bonded since too much oxide left. A similar phenomenon of distribution of oxide particles in the peripheral region is shown in Fig. 4(c) and (d). The pits in Figs. 3(d) and 4(d) indicate a serious wear of glass by the oxide particles. For most of the other specimens, glass fracture takes a big part of the interface and little aluminum residuals coexist. Different from metal-metal wire bonding where only metallic bonds are formed, ionic or metallic bonds might form among Al, Si and O for the Al-SiO_2 bonding [28,29]. The exact bond types at the bonding interface, however, need further studies.

To further confirm that the bright particles in the videos are oxides, Energy-dispersive X-ray spectroscopy (EDS) analysis was performed on those particles. An example is shown in Fig. 5. The EDS scan reveals the composition of the sample surface on the illustrated green line. In contrast to the Al and Si signals, which show a dramatic response, the oxygen signal is quite constant. It is indicated that both the surface and the particle have a similar content of oxygen. Since the substrate is made from silicon dioxide, it can be deduced that the particle is non-metallic and is an oxide particle.

3.3. Impact of process parameters

The process parameters including the normal force and the US power were varied (see Fig. 6) to investigate their impacts on the five areas including the contact area, friction area, stick area, microwelds area and oxides area. For convenience, only the oxides within the stick area are terminated as oxides area in this article. The impacts are compared in Fig. 6 that shows the changes of the five areas within the recording window over the process time.

When the US power keeps constant, the increase of normal force greatly enhances the contact, stick and microwelds areas within the

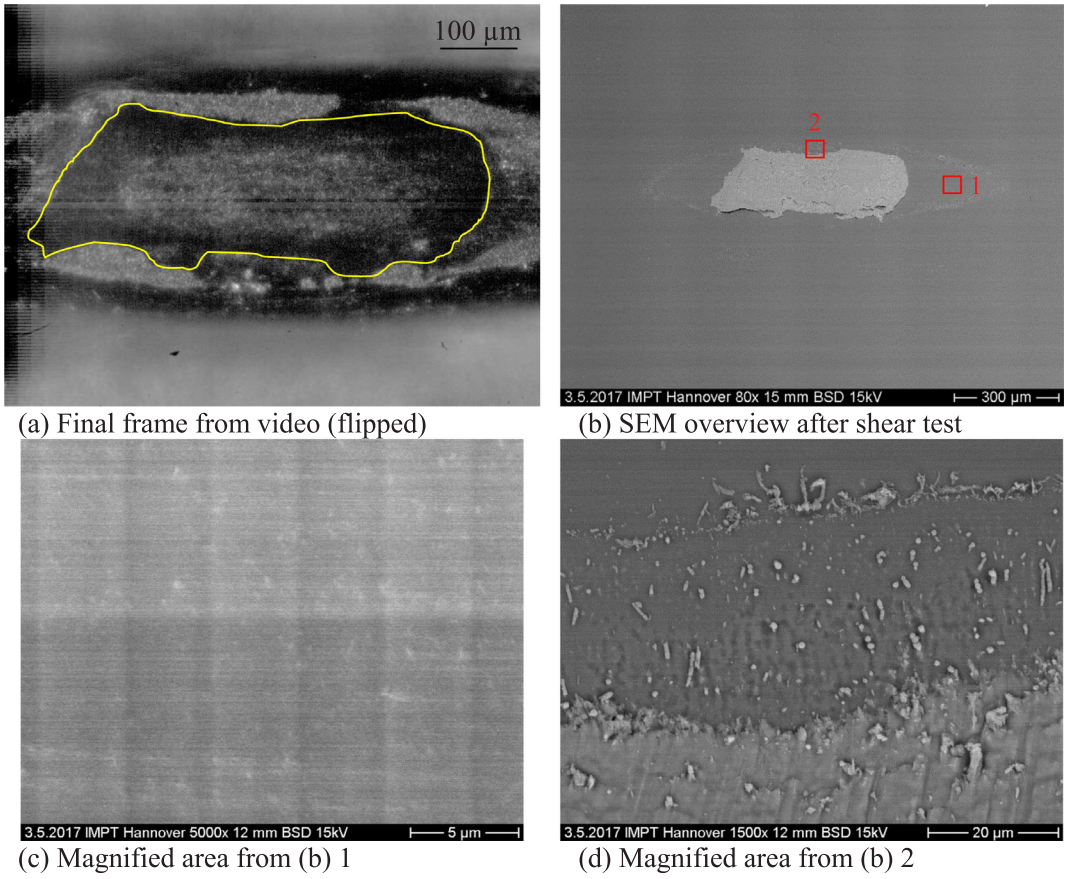

(a) Final frame from video (flipped) (b) SEM overview after shear test

(c) Magnified area from (b) 1 (d) Magnified area from (b) 2

Fig. 3. SEM observation of wire/glass interface for 5 N 1.3 W process.

testing range. The friction area increases as the increase of the normal force in the beginning stage, but soon decreases to a lower platform after the appearance of the stick area. When the normal force stays the same, the increase of US power significantly enlarges the contact and friction areas while the stick and microwelds areas might not be increased or even decreased (see Fig. 6(d)). This indicates that too much US power input would be detrimental to the microwelds formation as excessive vibration can cause the breakage of existing microwelds and prevent formation of new microwelds. If the US power is too small, however, little oxides can be removed and the growth of microwelds area gets limited. As a result, the UP power must be carefully selected so that the positive effect of vibration can be fully utilized. In addition, the transfer of US power to the bonding interface must be coupled with a corresponding normal force. When the force is comparably small, too large vibration amplitude is not beneficial for microwelds formation. When the force is too large, more oxides retain within the stick area since vibration is not sufficient for the removal of these oxides (see Fig. 6(b) and (e)). From all the figures, it can be seen that the growth of the contact and friction areas in the beginning is fast and becomes slower and slower in the latter stage. The formation of microwelds is slow in the beginning, becomes much faster shortly after the beginning stage under proper settings and gets slow again in the final stage.

An important prerequisite condition for microwelds formation is the removal of oxides. As a result, the self-cleaning efficiency of the bonding process is an important indication for the bonding quality. As shown in the images subtracted from the high-speed videos, the contact area outside of the stick area always showed a high brightness. Oxides could also flow back to the stick area if the local microwelds were broken, as shown in the upper-left potion of Fig. 2(e) and (f). Therefore, the microwelds area is considered as the oxide-free area in this work. The cleaning coefficient is then calculated as the ratio of microwelds area over contact area. The change of the cleaning coefficient over process time under different parameter settings are shown in Fig. 7. In the beginning stage of the bonding process, the cleaning coefficient was zero as no microwelds were formed. After 50–150 ms, a rapid increase of microwelds area was observed. After this stage, the increase became slower and finally reached a constant value.

The cleaning coefficient is determined by both the vibration and the continuous plastic deformation. As mentioned before, the vibration has both positive and negative effects on the microwelds (oxide-free area). Without US vibration, no microwelds can be formed. Excessive vibration, however, damages the existing microwelds and inhibit the formation of new microwelds. The contact area is determined by the continuous plastic deformation. For the 5 N 3.3 W process, the excessive vibration greatly influenced the formation of microwelds. Therefore, the cleaning coefficient of this process is the smallest. As the US power decreased, the negative effect of vibration on microwelds became less significant and more microwelds could thus be formed. In addition to the smaller contact area, the 5 N 2.4 W process has a large cleaning coefficient and the cleaning coefficient of the 5 N 1.3 W process is even larger. As the normal force increased to 6 N, the negative effect of US vibration (2.1 W) on microwelds was less significant than that of the 5 N 2.4 W process. Due to the large contact area, the cleaning coefficient of the 6 N 2.1 W process is slightly smaller than that of the 5 N 2.4 W process. When the normal force decreased to 4 N, an US power of 1.4 W still seems to be very high. The excessive vibration inhibited the formation of microwelds and resulted in a low cleaning coefficient. As it has a smaller contact area, its cleaning coefficient is larger than that of the 6 N 2.1 W process. Naturally, the cleaning coefficient is not the only indicator of the bonding quality. When selecting process parameters, their impacts on both the cleaning coefficient and the contact area must be taken into consideration.

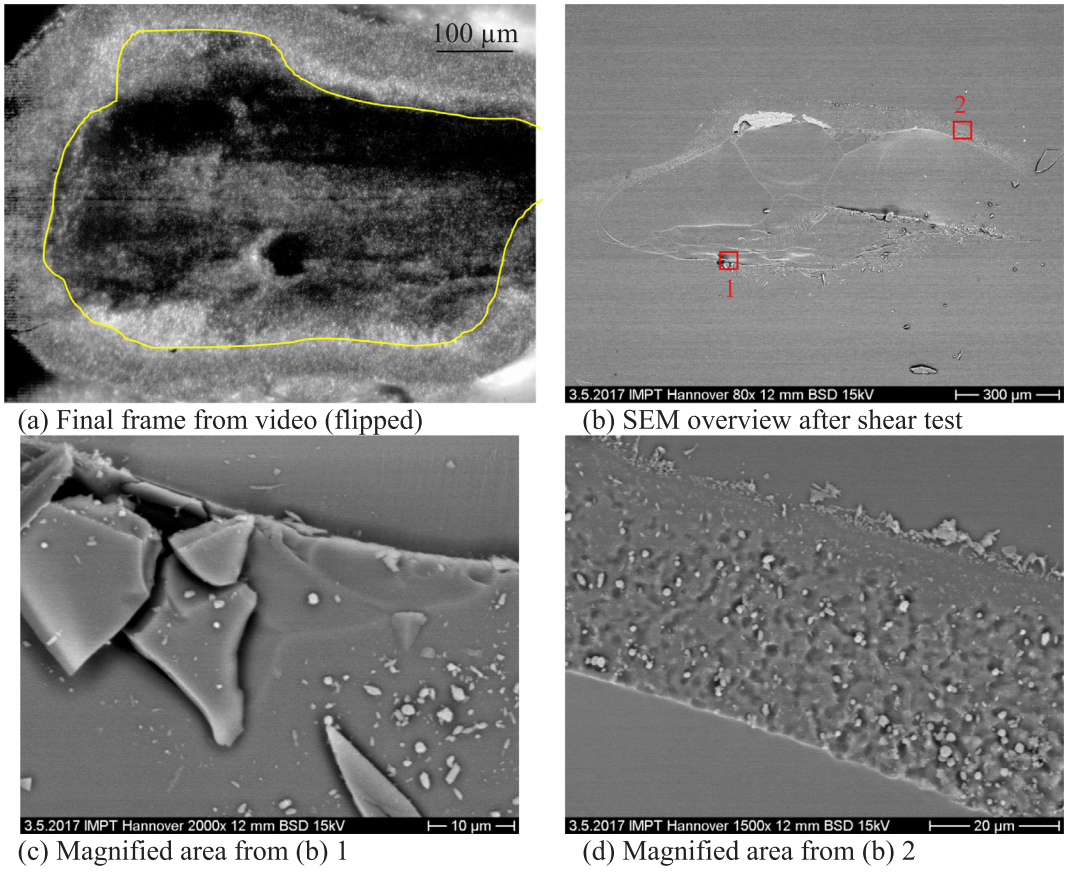

(a) Final frame from video (flipped)
(b) SEM overview after shear test
(c) Magnified area from (b) 1
(d) Magnified area from (b) 2

Fig. 4. SEM observation of wire/glass interface for 6 N 2.1 W process.

3.4. The prediction of shear strength

Since the shear strength of a bond is determined by microwelds, the detection and quantification of the microwelds area in the high-speed videos can be used to predict the shear strength of the bonds. The microwelds areas as recorded by the high-speed observation system have been illustrated in Fig. 6. All the specimens were shear tested. Due to the very weak connection, the shear strength of the specimens under 5 N 3.3 W were not detectable. The shear strengths and the calculated ultimate shear stress of microwelds for the other specimens are shown in Table 1. The values of the ultimate shear stress are around 95 MPa, which is larger than that for Al-Al bonding (58.31 MPa) [11]. The difference is mainly caused by the different materials.

To more accurately validate the microwelds areas from the videos, the bonding interfaces of the specimens were inspected by a laser confocal microscope Keyence VK-9700. Fig. 8 shows the interfaces of two specimens and the white flat areas are microwelds areas. As shown in Table 1, the ultimate shear stress (95.72 ± 2.21 MPa) calculated from the videos is quite close to that (94.56 ± 2.35 MPa) calculated from the microscopic images. Therefore, the high-speed observation can be used for long-term quality monitor and control of the metal-glass bonding process.

3.5. Moving of oxide particles

The two end areas have been real-time observed as well. Due to the uneven distribution of normal stress, the friction force was much smaller at the boundary area of the contact, especially at the beginning stage. Since the stress within these regions was too small to break the oxide scale in the beginning stage, these regions showed a dark contrast to the inner areas where the oxide scale has been broken up into particles and a high brightness has been obtained. As a result, the moving of bright oxide particles from the bright inner area to the dark peripheral region was able to be observed.

Part of the oxides moving is shown in Fig. 9 (the video can be found in the Supplementary material). In Fig. 9(a), a large amount of oxides accumulated in the red circle. After ~25 ms, most of the oxide particles in the red circle moved to the blue elliptic in Fig. 9(c). A group of moving particles was captured in the green elliptic in Fig. 9(b). In addition, the motion speed of the particles was much higher than the material flow speed. The same as in the end areas, the removal of oxide particles to the outside of the contact in the middle contact area can be observed when the material flow speed was close to zero. Both of these phenomena proved that the vibration plays a significant role in the oxide removal process.

4. Conclusion

In this work, via a real-time observation of metal-glass bonding, three out of the four phases – Pre-deformation and activation of US vibration, Friction and Softening, were detected for the first time from a 2-D point of view. The findings are summarized as the following:

- During the bonding process, five different areas including the contact area, friction area, stick area, microwelds area and oxides area were captured. The stick area and microwelds area started from the central contact region and extends outwards.
- The co-existence of friction (friction area), macroscopic expansion of wire (contact area) and microwelds formation (microwelds area) confirmed the overlap characteristic of the friction and softening phases.
- The oxides were first broken into small particles after the detachment from the metal surface. Most of them were then transported to the peripheral contact region.

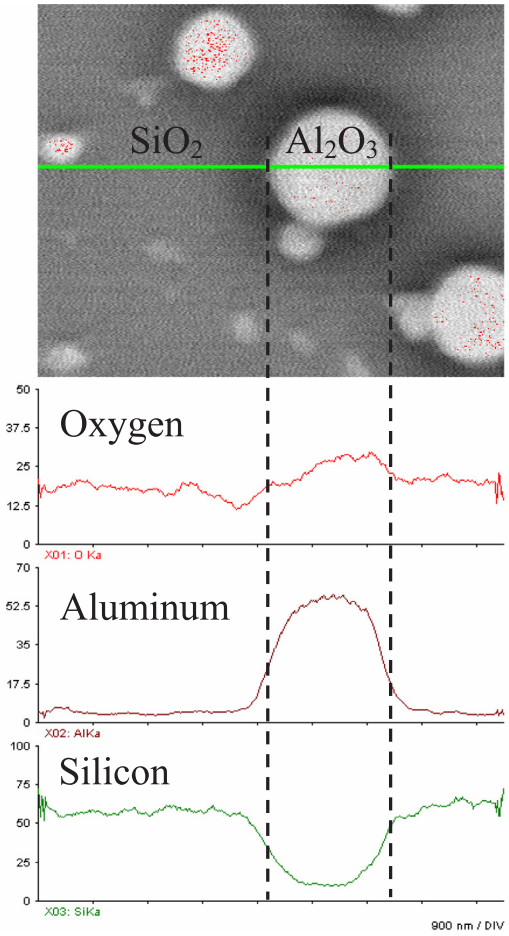

Fig. 5. An EDS line scan of a particle.

- The transportation of oxides was captured and it was verified to be caused by both the material flow and vibration.
- The normal force and US power interactively influence the contact area, friction area, stick area, microwelds area and oxides area. In general, a large force and US power increase the contact, stick and microwelds areas. A too high US power can cause the breakage of the existing microwelds and inhibit further formation of new microwelds.
- The cleaning coefficient increases rapidly in the middle stage of the bonding processes. It is greatly influenced by the normal force and US power.
- Via the high-speed observations, the ultimate shear stress of metal-glass microwelds was calculated to be 95.72 ± 2.21 MPa, which can be used to predict the shear strength and optimize the process

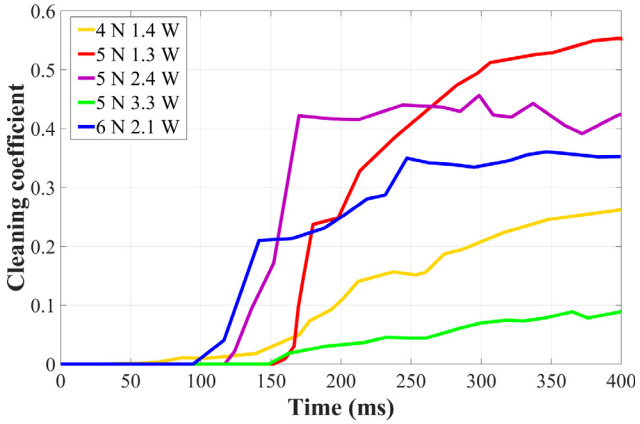

Fig. 7. Impact of process parameters on cleaning coefficient within contact area.

Table 1
Microwelds area and shear strength.

Specimen	Shear force (N)	Microwelds area (μm²)		Ultimate shear stress (MPa)	
		Video	Microscope	Video	Microscope
4 N, 1.4 W	3.77	39239.09	38761.19	96.08	97.26
5 N, 1.3 W	8.09	82373.17	86776.66	98.21	93.23
5 N, 2.4 W	7.84	84447.40	85173.07	92.84	92.05
6 N, 2.1 W	11.22	117183.66*	117269.01	95.75	95.68

* This value is smaller than the real value since the final microwelds area exceeds the recording window. According to the microscope image, an additional 14079.11 μm² shall be added.

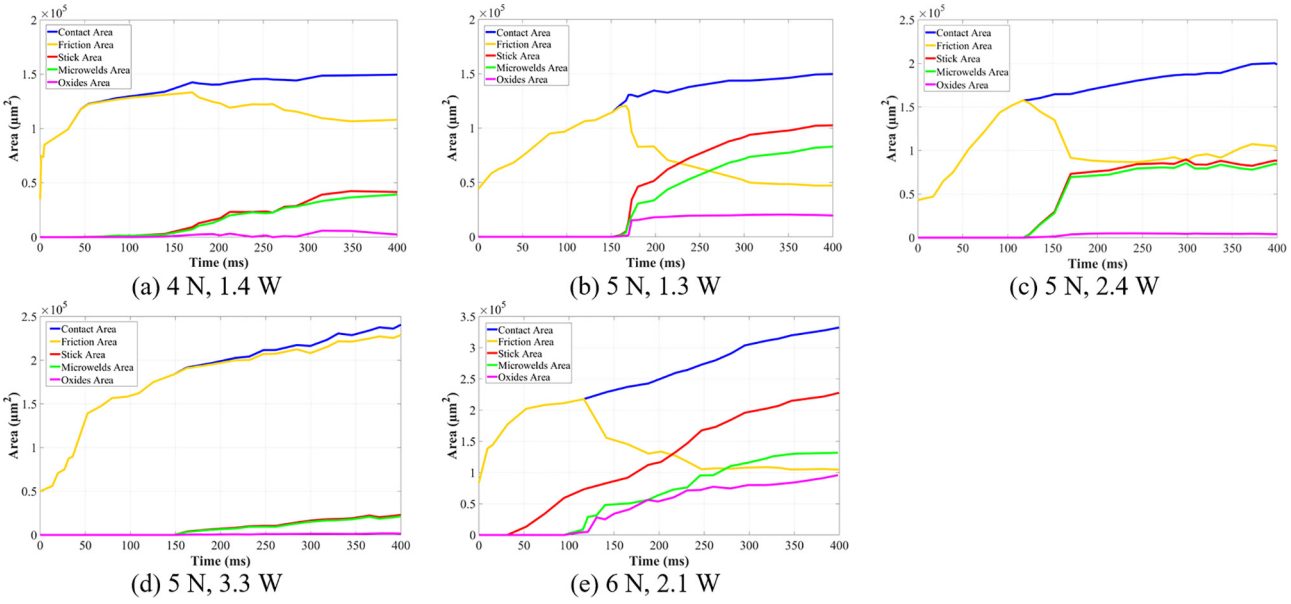

Fig. 6. Growth of contact, friction, stick, microwelds and oxides area under different settings.

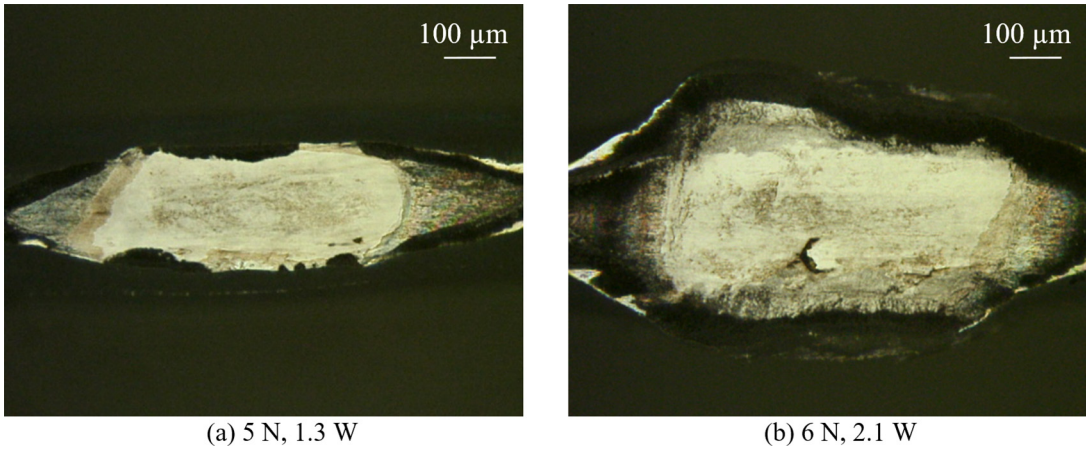

Fig. 8. The bonding interface by Keyence VK-9700.

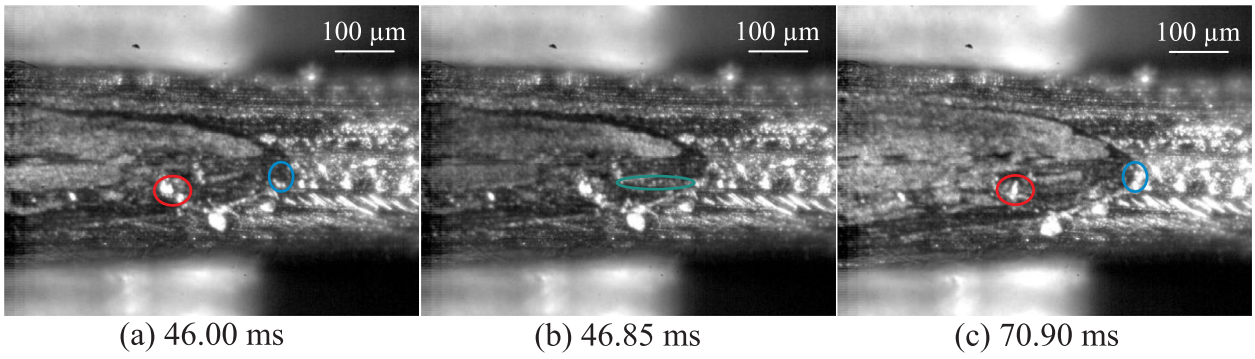

Fig. 9. Moving of oxide particles under 6 N, 2.0 W.

parameters.

Acknowledgement

This work is supported by DFG (Deutsche Forschungsgemeinschaft) programm [TW75/8-1| WA 564/40-1|WU 558/11-1]. Appreciations are given to Hesse Mechatronics GmbH for providing the bonding head HBK05.

Appendix A. Supplementary data

Supplementary data to this article can be found online at https://doi.org/10.1016/j.mseb.2018.11.010.

References

[1] G.G. Harman, Wire Bonding in Microelectronics, third ed., McGraw-Hill, New York, 2010.
[2] Y. Long, J. Twiefel, J. Wallaschek, A review on the mechanisms of ultrasonic wedge-wedge bonding, J. Mater. Process. Technol. 245 (2017) 241–258.
[3] H. Gaul, M. Schneider-Ramelow, K.D. Lang, H. Reichl, Predicting the shear strength of a wire bond using laser vibration measurements, IEEE Electron. Syst.-Integ. Technol. Conf. (2006) 719–725.
[4] A. Unger, W. Sextro, S. Althoff, T. Meyer, K. Neumann, R.F. Reinhart, M. Brökelmann, K. Guth, D. Bolowski, Data-driven modeling of the ultrasonic softening effect for robust copper wire bonding, Int. Conf. Integ. Power Syst. (2014) 1–11.
[5] A. Unger, W. Sextro, S. Althoff, P. Eichwald, T. Meyer, F. Eacock, M. Brökelmann, M. Hunstig, D. Bolowski, K. Guth, Experimental and numerical simulation study of pre-deformed heavy copper wire wedge bonds, Int. Symp. Microelectron. (2014) 289–294.
[6] M. Mayer, J. Schwizer, O. Paul, D. Bolliger, H. Baltes, In situ ultrasonic stress measurements during ball bonding using integrated piezoresistive microsensors, Proc. Intersociety Electron. Pack. Conf. (1999) 973–978.
[7] H. Gaul, A. Shah, M. Mayer, Y. Zhou, M. Schneider-Ramelow, H. Reichl, The ultrasonic wedge/wedge bonding process investigated using in situ real-time amplitudes from laser vibrometer and integrated force sensor, Microelectron. Eng. 87 (2010) 537–542.
[8] A. Unger, W. Sextro, T. Meyer, P. Eichwald, S. Althoff, F. Eacock, M. Brökelmann, M. Hunstig, K. Guth, Modeling of the stick-slip effect in heavy copper wire bonding to determine and reduce tool wear, Electron. Pack. Technol. Conf. (2015) 1–4.
[9] H. Gaul, M. Schneider-Ramelow, H. Reichl, Analysis of the friction processes in ultrasonic wedge/wedge-bonding, Microsys. Technol. 15 (2009) 771–775.
[10] Y. Long, J. Twiefel, J. Roth, J. Wallaschek, Real-time observation of interface relative motion during ultrasonic wedge-wedge bonding process, Int. Symp. Microelectron. (2015) 419–424.
[11] Y. Long, F. Schneider, C. Li, J. Hermsdorf, J. Twiefel, J. Wallaschek, Quantification of the energy flows during ultrasonic wire bonding under different process parameters, Int. J. Pr. Eng. Man.-GT (2018) accepted.
[12] Y. Long, F. Dencker, F. Schneider, B. Emde, C. Li, J. Hermsdorf, M. Wurz, J. Twiefel, Investigations on the oxide removal mechanism during ultrasonic wedge-wedge bonding process, Electron. Pack. Technol. Conf. (2016) 405–410.
[13] Y. Long, F. Dencker, M. Wurz, A. Feldhoff, J. Twiefel, A deeper understanding on the motion behaviors of wire during ultrasonic wedge-wedge bonding process, Int. Symp. Microelectron. (2016) 427–432.
[14] Y. Zhou, X. Li, N.J. Noolu, A footprint study of bond initiation in gold wire crescent bonding, IEEE Trans. Compon. Packag. Technol. 28 (2005) 810–816.
[15] I. Lum, M. Mayer, Y. Zhou, Footprint study of ultrasonic wedge-bonding with aluminum wire on copper substrate, J. Electron. Mater. 35 (2006) 433–442.
[16] H. Seppänen, R. Kurppa, A. Meriläinen, E. Hæggström, Real time contactresistance measurement to determine when microwelds start to form duringultrasonic wire bonding, Microelectron. Eng. 104 (2013) 114–119.
[17] H. Ji, M. Li, Y. Kweon, W. Chang, C. Wang, Observation of ultrasonic Al-Si wire wedge bond interface using high resolution transmission electron microscope, Int. Conf. Electron. Pack. Technol. (2007) 1–4.
[18] H. Ji, M. Li, J.-M. Kim, D.-W. Kim, C. Wang, Nano features of Al/Au ultrasonic bond interface observed by high resolution transmission electron microscopy, Mater. Charact. 59 (2008) 1419–1424.
[19] U. Geissler, J. Funck, M. Schneider-Ramelow, H.-J. Engelmann, I. Rooch, W.H. Müller, H. Reichl, Interface formation in the US-wedge/wedge-bond process of AlSi1/CuNiAu contacts, J. Electron. Mater. 40 (2011) 239–246.
[20] M. Maeda, Y. Yoneshima, H. Kitamura, K. Yamane, Y. Takahashi, Deformation behavior of thick aluminum wire during ultrasonic bonding, Mater. Trans. JIM 54 (2013) 916–921.
[21] M. Maeda, Y. Takahashi, Deformation and bond-area expansion of thick aluminum wire during ultrasonic bonding, Trans. JWRI 42 (2013) 15–20.
[22] I. Ille, J. Twiefel, Model-based feedback control of an ultrasonic transducer for

ultrasonic assisted turning using a novel digital controller, Phys. Procedia 70 (2015) 63–67.
[23] Y. Long, F. Dencker, A. Isaak, J. Hermsdorf, M. Wurz, J. Twiefel, Self-cleaning mechanisms in ultrasonic bonding of Al wire, J. Mater. Process. Technol. 258 (2018) 58–66.
[24] F. Blaha, B. Langenecker, Plastizitätsuntersuchungen von metallkristallen in ultraschallfeld, Acta Metall. 7 (1959) 93–100.
[25] B. Langenecker, Effects of ultrasound on deformation characteristics of metals, IEEE Trans. Sonics Ultrason. 13 (1966) 1–8.
[26] M. Maeda, K. Yamane, S. Matsusaka, Y. Takahashi, Relation between vibration of wedge-tool and adhesion of wire to substrate during ultrasonic bonding, Q. J. Japan Weld. Soc. 27 (2009) 200s–203s.
[27] Y. Long, B. He, W. Cui, X. Zhuang, J. Twiefel, Molecular dynamics simulation of microwelds formation and breakage during ultrasonic copper wire bonding, Electron. Compon. Technol. Conf. 1 (2018) 1434–1439.
[28] K. Prabriputaloong, M.R. Piggott, The reaction between silica and aluminum, J. Electrochem. Soc. 121 (1974) 430–434.
[29] N. Yoshikawa, H. Wang, S. Taniguchi, Application of microwave heating to reaction between soda-lime glass and liquid al for fabrication of composite materials, Mater. Trans. 50 (2009) 1174–1178.